



Improving Deep Learning-Based Digital Image Correlation with Domain Decomposition Method

Y. Chi¹ · Y. Liu¹ · B. Pan¹

Received: 17 August 2023 / Accepted: 6 February 2024 / Published online: 12 March 2024
© Society for Experimental Mechanics 2024

Abstract

Background Deep learning-based digital image correlation (DL-based DIC) has gained increasing attention in the last two years. However, existing DL-based DIC algorithms are impractical because their application scenarios are mostly limited to small deformations.

Objective To enable the use of DL-based DIC in real-world general experimental mechanics scenarios that would involve large deformations and rotations, we propose to improve DL-based DIC with the domain decomposition method (DDM).

Methods In the improved method, the region of interest is divided into subimages, and subimages are pre-aligned using the preregistered control points to effectively eliminate the large deformation components. The residual deformations in each subimage are small and limited, which can be well extracted using existing DL-based DIC methods.

Results Through synthesized and real-world experiments, the improved DL-based DIC method can achieve high-accuracy pixelwise matching in practical applications with strong robustness and high computational efficiency.

Conclusions The improved DL-based DIC combines the advantages of traditional and DL-based DIC methods but overcomes the limitations, greatly improving the robustness and applicability of existing DL-based methods.

Keywords Digital image correlation · Deep learning · Domain decomposition method

Introduction

Digital Image Correlation (DIC) is a non-contact, full-field deformation measurement technique that extracts surface deformation by analyzing digital images of an object acquired at different states [1–3]. As a revolutionary photo-mechanics technique, DIC has been widely used in various scientific disciplines and engineering practices. Traditional DIC algorithms, in essence, are physical model-based numerical optimization methods. They either use shape functions to describe local deformation around discrete calculation points [4, 5] (i.e., local DIC) or adopt mesh to model deformation within the region of interest [6, 7] (i.e., global DIC). Despite the widespread use of these traditional DIC algorithms, they are incapable of obtaining accurate pixelwise dense deformation fields, especially for

complex deformation fields. It is for sure that one would use more calculation points in local DIC and finer mesh in Global DIC (known as h-refinement), or use models with more parameters like 2nd-order shape function [5] in local DIC and higher-order elements [8, 9] in global DIC (known as p-refinement). However, proper selection of the model parameters (subset size, grid step, shape function, element type, etc.) is generally considered to be tricky, and these model parameters still have limited description capacity of deformation. Let alone that model with higher description capacity usually contains more parameters to be optimized and requires hugely increased computation costs.

In recent years, widely successful applications of deep learning (DL) methods in various fields have inspired the introduction of DL methods into DIC. Different than the physical model-based methods that rely on explicit parameters, DL-based DIC methods characterize deformations through an implicit neural network model that contains a large number of parameters [10]. Therefore, it can handle more complex deformations with implicit neural representation and achieve pixelwise dense results without the need for model parameter selection. Specifically, Boukhtache et.al

✉ B. Pan
panb@buaa.edu.cn

¹ National Key Laboratory of Strength and Structural Integrity, School of Aeronautic Science and Engineering, Beihang University, Beijing 100191, China

first introduced DL into DIC and proposed the StrainNet [11, 12] based on the U-Net [13] architecture. Detailed comparison with the existing optical flow frameworks such as FlowNet [14] and PWC-Net [15] demonstrated that StrainNet achieves higher measurement accuracy in a specific displacement range (less than 1 pixel), proving the feasibility of DL-based DIC methods. However, the measurement range of a DL-based method is limited by the generalization ability, which is affected by the covered displacement range of the dataset. If the measured displacement exceeds the range, the results may be unreliable or even erroneous.

To enhance the practicality of DL-based DIC method in handling larger displacement and diverse speckle patterns, two different ways can be adopted. The first straightforward approach is to use larger datasets covering wider varieties of deformations to gain higher generalization. For example, DeepDIC [16] uses grid deformation for datasets generation and DIC-Net [17] adopts the Hermite basis function to improve the continuity and enrich deformation modes in datasets. Also, the maximum displacement range is increased up to 16 pixels in DICNet [18]. However, increasing the dataset coverage cannot break the limitation once and for all. Another approach involves cascading different networks to handle different displacement ranges, adopting the idea of coarse and fine search. For example, CNN-SDM [19] proposes to cascade two neural networks to extract displacement of 0.1-pixel and 0.01-pixel levels respectively. Also, DVC-Net [20] uses three cascaded fully connected networks for integer pixel, sub-pixel, and sub-region denoising, which has been successfully applied in measuring cell traction force [21]. The same architecture with three fully connected networks is also adopted for 2D DIC [22]. R³-DICnet [23] adopted the base architecture of LiteFlowNet [24] and the similar gate recurrent unit (GRU) in RAFT [25] and trained on a dataset consisting of both small (5 pixels) and large displacement (up to 30 pixels), achieving a capability of large displacement measurement up to 30 pixels. Recently, for 3D-DIC measurement, StrainNet-3D [26] uses the affine transformation to pre-register the stereo image pair and uses two networks to extract subpixel displacements and refine displacements respectively, making it suitable for handling perspective deformations.

Existing research mainly focuses on improving measuring accuracy by enriching the dataset, optimizing network structure, or employing a pyramid strategy to integrate multi-scale results. After fine-tuning, these DL-based methods can achieve results with comparable accuracy to traditional methods in the covered displacement range. However, in real-world application scenarios, the practicality of DL-based methods is limited by two main factors, namely, the coverage of datasets (including the displacement range and the diversity of speckle pattern) and the compatibility of the input image sizes. Firstly, displacements often reach tens or

even hundreds of pixels in real-world applications. Also, when high-resolution cameras are used, the displacements would be larger, which could be far beyond the range of datasets in existing DL-based methods, among which the maximum displacement is only 30 pixels [23]. Although expanding the coverage of a dataset can further improve generalization, it is impractical to encompass all possible testing scenarios with unknown large displacements. Moreover, a network trained on a dataset with larger displacements would show increased random errors when used to measure small displacements, which greatly prevents the practical application of DL-based DIC methods. Secondly, the sizes of input images are variable. To accommodate images with different resolutions, networks with fixed input sizes, as in [16, 20–22], often employ scaling or splitting strategies. However, scaling may affect the output accuracy, and splitting may yield unreliable results near the image boundaries as the tracked pixel may extend beyond the subimage's boundaries. For those U-Net-based networks [11, 12, 17, 26], although they do not strictly limit the input size, the measurable range is still limited by the receptive field of the network structure. A larger receptive field requires larger input images and deeper convolution layers, leading to higher training costs. Additionally, the difference in size between testing and training images would also affect output accuracy. In conclusion, to improve the practicality and generalization of DL-based DIC methods, one can continuously expand the dataset to cover different displacement ranges and various speckle patterns and can develop better network structures like RAFT [25] in optical flow tasks that have a global receptive field. It is important to note that these limits are inherent to data-driven DL methods. The marginal cost of retraining networks and modification is relatively high to further improve the performance.

Considering the locality of the DIC problem that the results of a point do not affect the results of other points, which is the fundamental logic of local DIC, this work adopts the idea of domain decomposition method (DDM) [27–29] to extend the measurement range of existing DL-based DIC methods without modification or retraining and make them generally applicable in practical measurements. The proposed method decomposes the DIC (or image matching) problem into two stages: 1) global large deformation (large displacement and rotation) removal, and 2) local small deformation refinement. In the global stage, the region of interest (ROI) is divided into subimages of a specific size using predefined control points. The deformed subimages are then pre-aligned using the transform calculated by the control points whose initial values are estimated using the method described in Ref [30]. After that, the residual displacements in deformed subimages are small and limited, resulting in local problems with a fixed image size and limited displacement range. The local problems are suitable for

the existing DL-based DIC method to accurately extract the residual displacement components. Note that, the subimage size can be changed according to the training image size to achieve better accuracy when different DL-based DIC networks are used. By merging the preregistered large components with the small components obtained by DL methods, refined full-field displacement fields can be obtained. The proposed method combines the advantages of traditional and DL-based DIC methods, thus can handle large displacements without sacrificing accuracy in small displacements, greatly improving the practicality and robustness of DL-based DIC methods.

The rest of this paper is organized as follows. Section "Improved DL-based DIC method" introduces the principle of the improved DL-based DIC method with DDM. In Section "Experiments", a validation experiment is demonstrated to show the effectiveness and accuracy of measurement. Additionally, a real experiment with large deformation is presented, proving the practicability of the proposed method. Section "Conclusions and future works" concludes this work and provides an outlook for future works.

Improved DL-based DIC method

Domain decomposition in DIC problem

DDM is a powerful numerical technique for solving finite element method (FEM) problems and has many applications in various scientific and engineering domains [27, 28]. It reduces the computational cost and memory requirement by dividing the domain into smaller subdomains and solving local problems on each subdomain. Thus, parallel computing can be performed to speed up the calculation. The key requirement of DDM is that the computation tasks within

each subdomain are relatively independent, and the solutions of each subdomain can be coordinated by exchanging boundary conditions.

In the DIC field, existing usage of DDM [29] focuses on solving the global equation with DDM method. However, the DIC problem has a strong locality that the displacement field requires only locally continuous without complex differential constraints and the matching results within a subdomain do not affect the results of other subdomains. Therefore, DDM could not only be used for solving the equation, but also be used to reform the calculation algorithm of DIC.

In this work, we adopt the idea of DDM to divide the ROI into small subimages and solve the local problem using DL-based DIC methods, then combine the local results of subimages into full-field results. To make full use of DL-based DIC methods, the subimages should meet the following requirements:

1. The displacement within each subimage should be small enough to be covered by the dataset. For example, when DICNet [18] where the maximum displacement is 16 pixels is used, the maximum displacement within the subimages should be smaller than 16 pixels, or the output results would be unreliable.
2. The size of subimages should be the same and small for higher performance with batch processing. Also, it should be properly chosen to ensure the compatibility with the DL-based DIC network.

To meet the first requirement, we proposed to pre-align the subimages with the control points pre-registered with the feature mesh interpolation method [30]. As shown in Fig. 1, the ROI is divided into subimages with control points evenly distributed with a step of 100 pixels. By using the 4 matched keypoint pairs, the perspective transformation between the

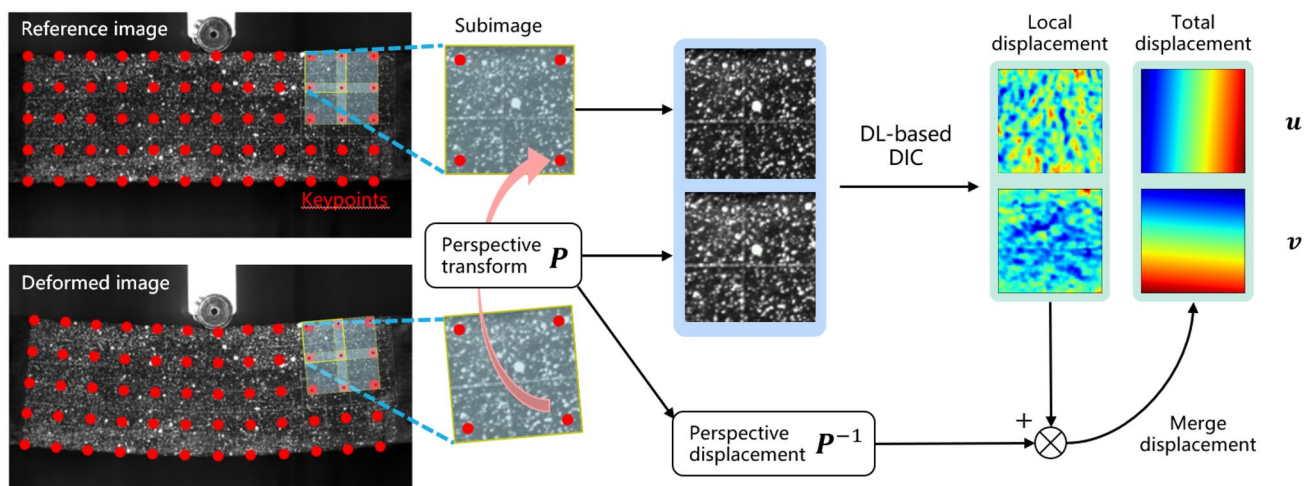


Fig. 1 Schematic diagram of DL-based DIC calculation aided by the domain decomposition method

reference and deformed subimages can be determined, representing the large deformation components of a subimage. To remove the large components, the deformed subimage is transformed into the reference frame with the obtained perspective transformation. Subsequently, the residual deformation components are small enough and limited in the subimage, thereby satisfying the first requirement.

As for the second requirement, the proposed DDM strategy transforms the global problem into a set of standardized local problems with fixed input sizes and limited deformations. These standardized problems can be well solved by existing DL-based methods. To accommodate potential large displacements without exceeding the subimage border, an extra border is added to the subimages. This border also allows for more reliable results in the overlapped region by weighting results of different subimages.

As for the selection of the keypoint step and border size, these parameters are determined based on the size of the ROI. The keypoint step is typically chosen as a factor of the ROI size, helping to avoid incorporating irrelevant background into subimages. The border size should exceed the potential displacement in the local problem and is usually chosen in the range of 10 to 20 pixels, depending on the magnitude of deformation and the measurement range of the DL-based DIC backend. For example, with an extra border of 14 pixels, the total size of a subimage is 128×128 pixels, which can be easily handled by most existing DL-based DIC networks.

DL-based DIC network for local displacement extraction

With the help of the DDM, the DIC backend could concentrate on the standardized local problem without the need for adaption and training for large displacements. The local problems can be effectively addressed by any existing DL-based DIC method mentioned before. However, in this work, we adopt an advanced optical flow network known as RAFT [25] to address the local problem. RAFT, with its larger receptive field and efficient utilization of prior information, outperforms existing U-Net-based networks. To enhance its performance for local problems with small input images (less than 256×256 pixels), several modifications have been made to the RAFT network, including refining the encoding module to capture more spatial information and reducing the channel number to achieve higher output resolution.

A dataset comprising various speckle patterns, deformations, noise levels, and lighting variations is generated and used for training the network. Consequently, the improved RAFT-based network achieves higher displacement registration accuracy for local problems and demonstrates better generalization ability. Nevertheless, we should note that this work focuses on the DDM strategy of extending the measurement range of DL-based DIC networks. Details and performance

evaluations of the proposed improved RAFT-based network would be presented in another work named “RAFT-DIC”.

Displacement field merging and boundary processing

With the DL-based DIC methods, the displacement field between reference subimages and deformed subimages can be efficiently calculated in batches using the powerful DL frameworks. However, the large displacement field obtained by the perspective transformation and the small displacement field obtained by DL-based methods cannot be directly added. They should be composed, as schematically shown in Fig. 2. The perspective transformation \mathbf{P} that transforms a control point (x'_i, y'_i) , $i = 1..4$ in the deformed subimage to its matched location in the reference subimage (x_i, y_i) can be expressed as:

$$\lambda \begin{pmatrix} x_i \\ y_i \\ 1 \end{pmatrix} = \mathbf{P} \begin{pmatrix} x'_i \\ y'_i \\ 1 \end{pmatrix}, i = 1..4 \quad (1)$$

where λ is an arbitrary scale factor and $(x_i, y_i, 1)^T$ is the homogeneous coordinates. The perspective matrix \mathbf{P} is 3×3 but only has 8 degrees of freedom due to the arbitrary scale factor. It can be uniquely solved with 4 control points as each point can provide 2 constraints.

For a point (x, y) in reference subimage, its corresponding point in the deformed subimage is (x_d, y_d) , and its coordinates after perspective transformation in the warped subimage is (x_w, y_w) . The local displacement between the warped location and the reference location is (u_l, v_l) , which is obtained from DL-based DIC methods. Then the corresponding point in the deformed subimage (x_d, y_d) is calculated using the inverse transform:

$$\lambda \begin{pmatrix} x_d \\ y_d \\ 1 \end{pmatrix} = \mathbf{P}^{-1} \begin{pmatrix} x + u_l \\ y + v_l \\ 1 \end{pmatrix} \quad (2)$$

The merged total displacement field within a subimage is obtained by subtracting the corresponding point in the deformed subimage from the reference subimage, which is expressed as:

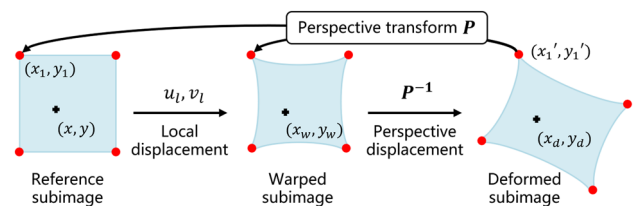


Fig. 2 Schematic diagram of displacement merging

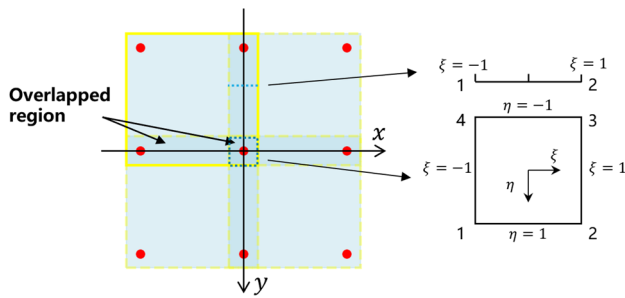


Fig. 3 Weights determination of the overlapped region

$$\begin{aligned} u &= x_d - x \\ v &= y_d - y \end{aligned} \tag{3}$$

Because a border was reserved when splitting the ROI, the overlapped region between subimages may contain more than one value from different subimages. Further processing of the overlapped region is required to obtain final results, as the data near the image edge in DL-based methods is less reliable. In this context, we use the weighted value of the overlapped region, with the weights determined by the shape function of linear elements in FEM. As shown in Fig. 3, in the overlapped region, we use the local normalized coordinates (ξ, η) to determine the weights. In an overlapped region of 2 subimages, the weights can be expressed as:

$$N_0 = \frac{1}{2}(1 - \xi), N_1 = \frac{1}{2}(1 + \xi) \tag{4}$$

where N_0 and N_1 are the weights of the two subimages. For the overlapped region of 4 subimages, the weights can be expressed as:

$$N_i = \frac{1}{4}(1 + \xi_i\xi)(1 + \eta_i\eta), i = 1..4 \tag{5}$$

The weighted average value of the overlapped region can be expressed as:

$$u = \sum_{i=1}^n u_i N_i \tag{6}$$

where n is the number of subimages in the overlapped region, u_i is the displacement values of the i -th subimage.

Experiments

Validation experiments using synthesized image

In this experiment, a synthesized image pair was generated and used to validate the proposed method. As shown in Fig. 4(c), an image with printed speckles is set as the reference image. A synthesized displacement field is applied to the reference image. The displacement field consists of a large and a small sinusoidal displacement components shown in Fig. 4(a) and (b), respectively, where the largest displacement reaches 115 pixels and the small sinusoidal displacement field is used for accuracy testing. The total displacement field is expressed as:

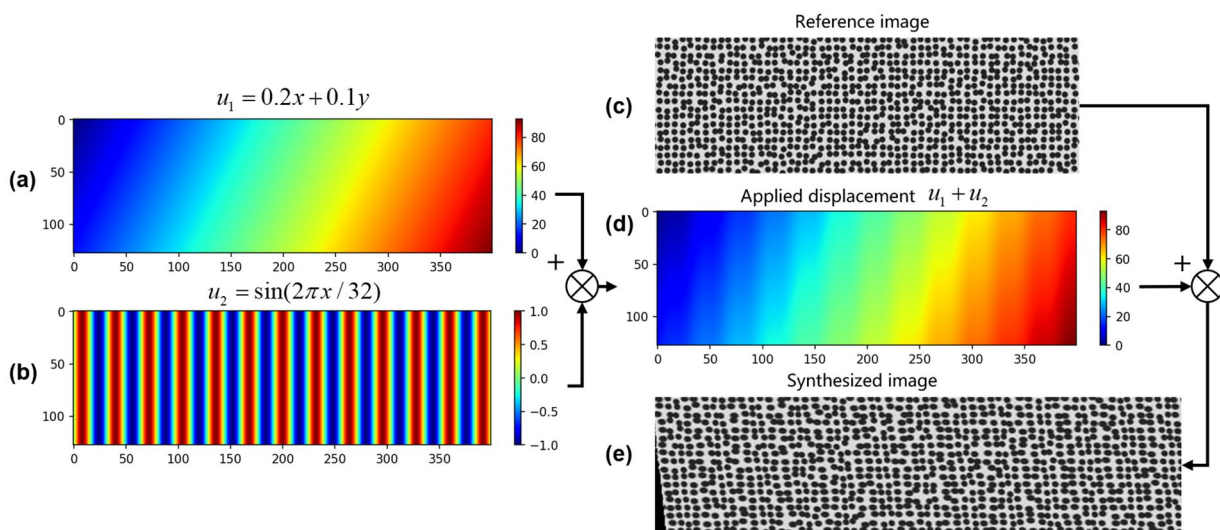


Fig. 4 (a) the large displacement components, (b) the sinusoidal small components, (c) the reference image, (d) the applied displacements and (e) the synthesized image

$$u(x, y) = 0.2x + 0.1y + \sin\left(\frac{2\pi x}{32}\right) \quad (7)$$

where, $u(x, y)$ is the horizontal displacement field, x and y are the image coordinates. Fig. 4(d) presents the applied displacement field, which is challenging for existing DL-based DIC methods to handle such large displacements. The frequency characteristic containing two frequency components also poses challenges for traditional local DIC algorithms with fixed subset sizes. Gaussian noise with a standard deviation of 3 gray levels is added to both the reference and synthesized deformed image, as shown in Fig. 4 (c) and (e). These images are used in subsequent experiments.

Considering the period of the applied small displacement field (32 pixels), we employ three subset sizes (31×31, 21×21, and 11×11 pixels) to demonstrate the performance of standard local DIC with different subset sizes. For comparison, the grid step in local DIC analysis is set to 1 pixel. The measured displacement fields and the measurement errors, obtained through local DIC method with different subset sizes and the improved DL-based DIC method, are shown in Fig. 5. When using a subset size of 31×31 pixels, which is close to the frequency of sinusoidal component, the measured displacement field fails to recognize this component, leading to undermatched errors. The magnitude of this undermatched error decreases as the subset size decreases

[31]. Specifically, adopting a subset size of 21×21 pixels reduces the undermatched error by approximately half, and the undermatched error can be further reduced with a smaller subset size (11×11 pixels). Nevertheless, further reduction in the subset size is not feasible due to the limitation of the average speckle size (7 pixels). During testing, attempts with smaller subsets, such as 9×9 or 7×7 pixels, proved unsuccessful in extracting the displacement field. This failure is attributed to the smaller subsets that lack sufficient unique speckle pattern information to reliably track the displacements. Moreover, the use of smaller subsets would introduce higher random errors, as indicated in previous studies [32].

For the improved DL-based DIC method, as marked in Fig. 6, the control points with a step of 50 pixels divide the ROI into 2×7 small subimages, and an extra border is set to 10 pixels. These parameters yield a series of subimages of 70×70 pixels. The results obtained with the proposed improved DL-based DIC method are shown in the last row of Fig. 5. The maximum error is less than 0.2 pixels, showing better performance (50% lower) than the local DIC method with an 11×11 subset size. Note that errors are still present, which can be attributed to the perspective warping and the inherent noise of the DL framework. Employing better dataset and network architecture would reduce this bias and further enhance accuracy. Compared with local DIC

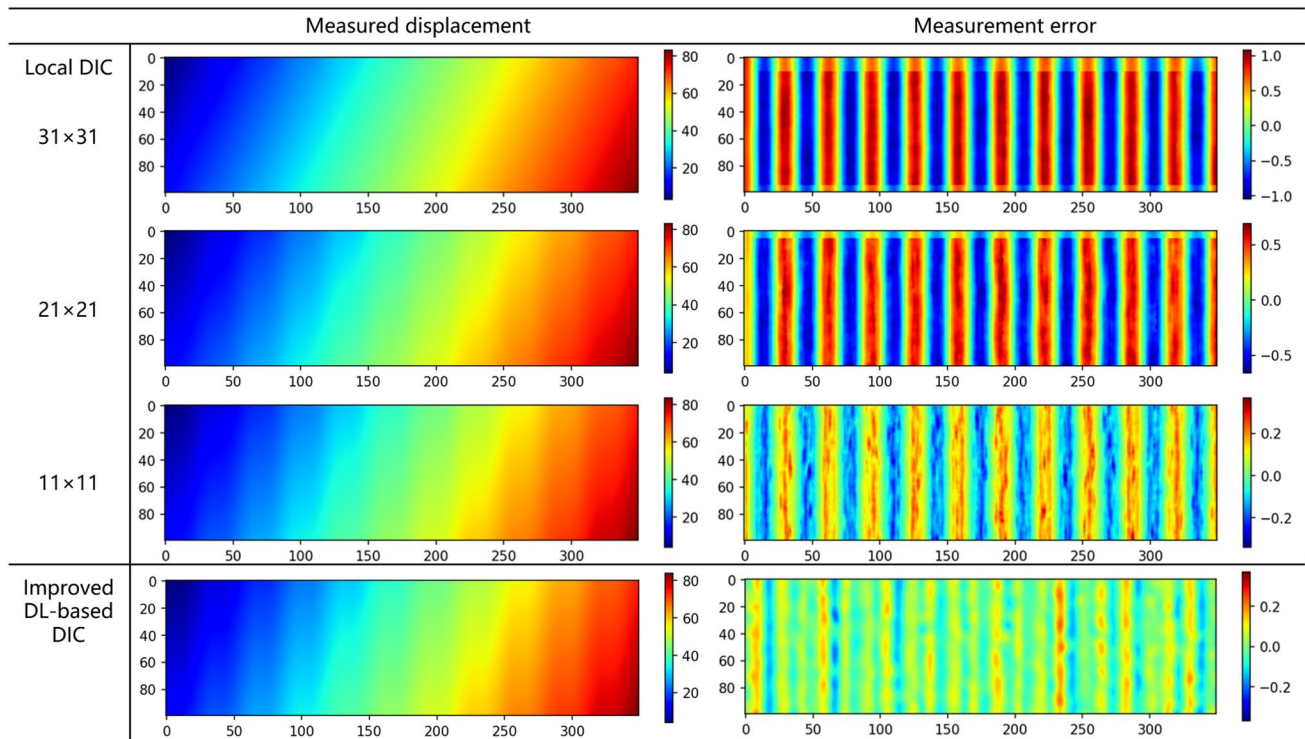
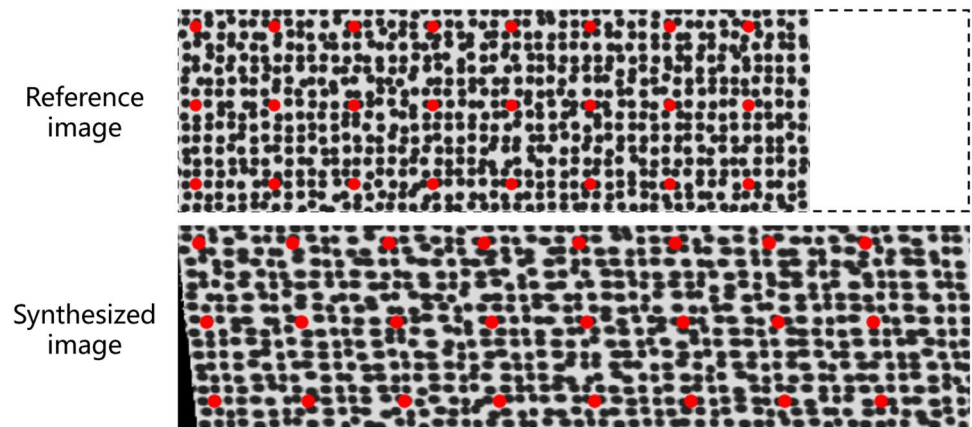


Fig. 5 Measured displacement and corresponding error maps using local DIC method with different subset sizes and the improved DL-based DIC method

Fig. 6 The reference image and the synthesized image marked with control points



methods, the proposed DDM strategy enables the DL-based DIC method to handle the large displacement without losing accuracy in high-frequency components. Moreover, it offers the advantage of accurate measurement without the need for parameter selection, providing a more convenient and efficient approach.

The measured components in two stages of the improved DL-based DIC method are shown in Fig. 7. In the first row, the large displacement component modeled by the perspective transformation of control points shows the same pattern with applied large displacement while the high-frequency components are screened out, while the difference of the large components are less than 1 pixel. Along with the small components, the maximum potential displacements in the local problems would be less than 2 pixels. The small displacement component is obtained after processing with the DL-based DIC methods. As shown in the second row

of Fig. 7, the same sinusoidal pattern is obtained, and the maximum displacement in the local stage is less than 1.5 pixels, indicating that the large displacement components are almost removed in the first stage. The differences in the small components exhibit a reverse pattern to that of the large components, resulting in a smaller overall error shown in the last row of Fig. 7. This demonstrates that the errors introduced by perspective transformation and the small components could be compensated by the DL-based methods. These results strongly prove that the proposed method can effectively separate different frequency components and can handle large displacements without sacrificing the accuracy of high-frequency fine displacement field.

For a comparative analysis with local DIC, Fig. 8 illustrates the error distributions of the two methods. In Fig. 8(a), the error distributions of the local DIC method with different subset sizes are presented. The bimodal distribution is

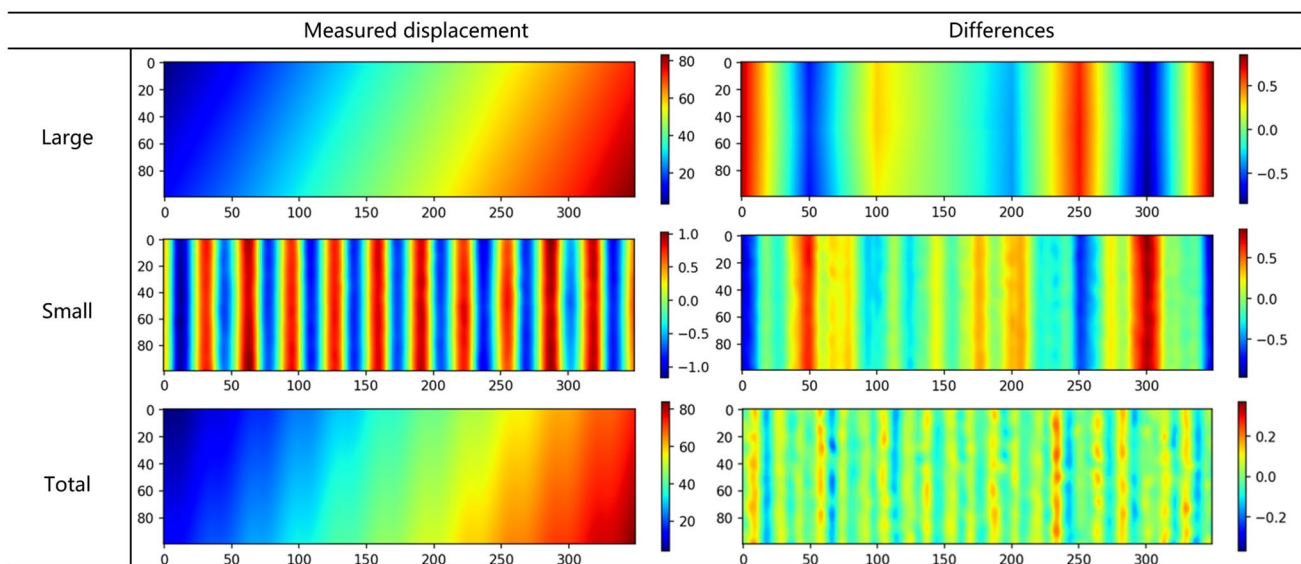


Fig. 7 Displacement components extracted by the improved DL-based DIC method, and the differences compared to the applied displacements

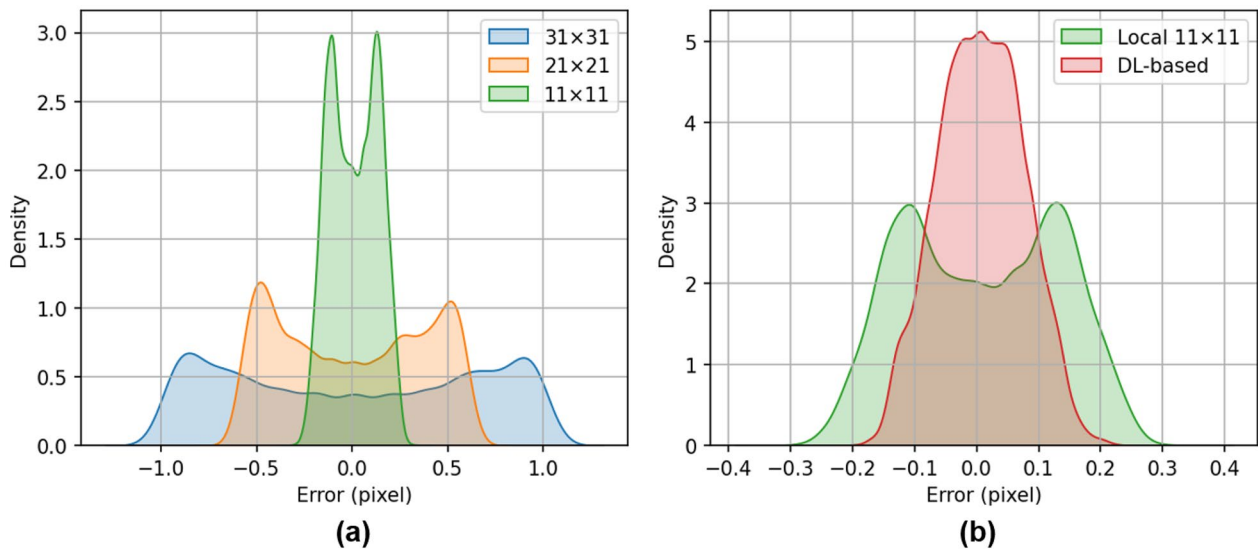


Fig. 8 (a) The error distribution of local DIC with different subset sizes, (b) the error distribution of local DIC with 11×11 pixels subset size and the improved DL-based DIC method

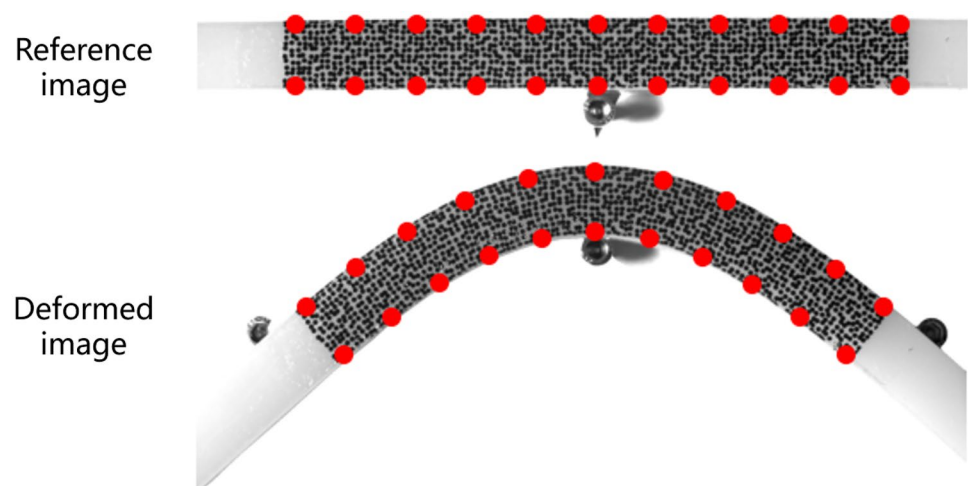
observed in the error distribution of local DIC, which arises from the undermatched error when measuring the sinusoidal displacement components. As the subset size decreases, the error distribution becomes more concentrated around zero. Fig. 8(b) shows the best case of local DIC (11×11 pixels) and the error distribution of the proposed method. Different from local DIC, the error of the DL-based DIC method shows a Gaussian distribution and higher concentration, owing to the inherent characteristics of neural networks. This highlights the ability of DL-based methods to accommodate various deformations without being significantly impacted by systematic undermatched errors. It is noteworthy that extracting different spatial frequencies using a standard DIC method with a fixed grid step can be challenging. Similarly, extracting high-frequency components using a predefined subset

size is also difficult. Results show that the proposed DDM strategy effectively measures the full-field complex displacements and achieves better accuracy than the standard local DIC method without requiring parameter selection, thus affirming the feasibility and effectiveness of the proposed method.

Large deformation measurement of a polyurethane beam

The proposed method with the DDM scheme was applied to measure the large deformation of a polyurethane beam. The beam is 20×40×500mm in size, and the ROI is on the narrow side with a size of 200×20mm. The speckle is pre-made by water transfer printing, which is soft and can stand

Fig. 9 The reference image and the deformed image with control points marked



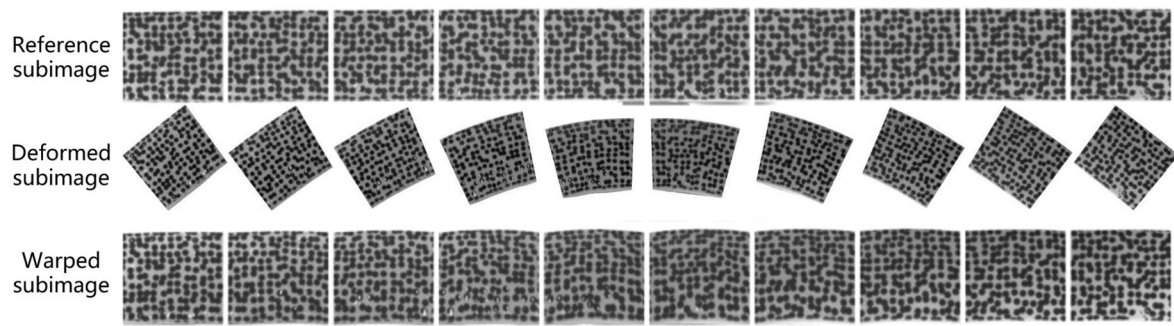


Fig. 10 Reference subimages and deformed subimages with inverse perspective transformation

with relatively large deformation without tearing. Images are captured by an industrial camera (FLIR-GS3-U3-28S4M-C, sensors: 1/1.2", active pixels:1928×1448) with an industrial lens (Computar, 25mm, F/1.4) facing the surface of the specimen. As shown in Fig. 9, the beam undergoes significant bending deformation with the applied displacement constraint. The preregistered control points divide the ROI into 10 subdomains along the horizontal direction. The grid step of control points is 150 pixels, and the border is chosen to be 20 pixels, therefore, each subimage has a size of 190×190 pixels. The maximum displacement of the imposed large deformation is about 360 pixels, exceeding the boundary of the subimage. This large deformation cannot be directly processed by the existing DL-based methods.

With the proposed method, deformed subimages are preregistered by the control points and warped back using the inverse perspective transform. In Fig. 10, the first row shows the reference subimages while the second rows show the corresponding deformed subimages. After removing large deformation with perspective transformation, the warped deformed subimages are shown in the last row of Fig. 10. It is evident that the large deformation has been effectively removed, resulting in a much smaller residual

deformation. Through the proposed method, the obtained local problems shown in Fig. 10 are much easier in comparison to the original problems that contained large displacement components.

The subimages with the same size are batch-processed using the improved DL-based methods. To briefly present the result details, only the data within the range of 400 to 800 pixels of the extracted vertical displacement field are shown in Fig. 11(a) and (b). The different perspective transformations in subimages result in discontinuities as marked in Fig. 11(a). However, this discontinuity is effectively addressed by DL-based DIC methods. The merged displacement field is presented in Fig. 11(c), where the discontinuities have been effectively compensated. The subtraction of the merged field and the large component, i.e., the additive small component, is shown in Fig. 11(d). Compared with Fig. 11(b), it is crucial to note that the merging process is not a simple addition, as it would lead to a loss in accuracy. As shown in Fig. 11(b), the maximum local displacement is less than 1 pixel, but it could compensate more as shown in Fig. 11(d) after the inverse perspective transformation, which further demonstrates the effectiveness of the proposed DDM strategy.

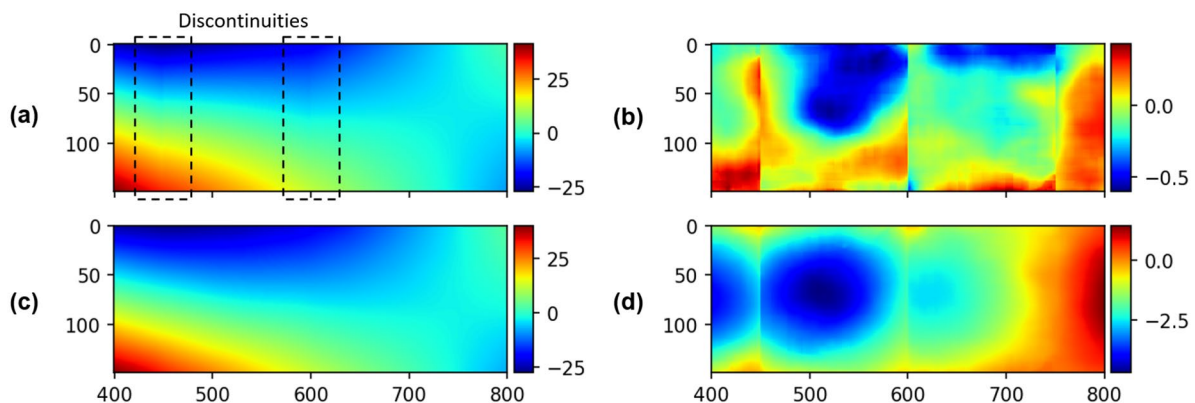


Fig. 11 (a) The extracted large component and (b) the small component of V field, (c) the merged total V field, and (d) the additive small component of V field

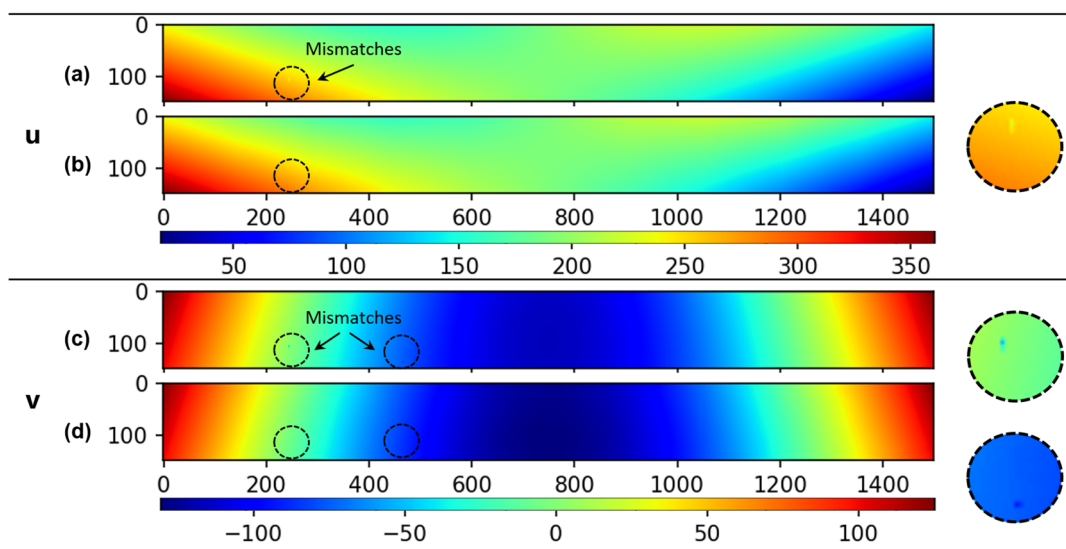


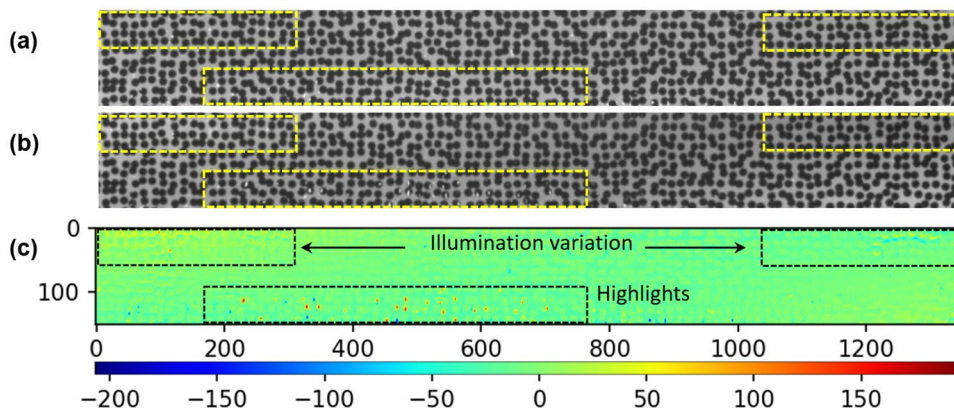
Fig. 12 Displacement field of different methods: (a) U field of DIC and (b) the proposed method, (c) V field of DIC and (d) the proposed method

After merging the results of the DL-based method and the field of inverse perspective transformation, the total displacement fields of U and V are shown in Fig. 12(b) and (d). Despite the largest displacement exceeding 360 pixels, the improved DL-based DIC method perfectly recovers the large deformation of the polyurethane beam. For comparison, the results of the standard local DIC method with subset size of 31×31 pixels and 1 pixel grid step are shown in Fig. 12(a) and (c). The results of the two methods are mostly identical, except for some mismatches, which have been marked and zoomed in for closer examination. These mismatches are inevitable in real-world experiments due to the highlights, noises, cracks, etc. However, in the proposed methods, the results are smooth and have no mismatches in the same region where highlights exist, as demonstrated below. It's noteworthy that this task is a big challenge for any other DL-based method, even for the most advanced optical flow algorithm like RAFT. Moreover, the ROI is 150×1500 pixels,

which took more than 3s for the advanced parallel local DIC [30] to compute the pixelwise results while the proposed methods took only 228ms, with 78ms used for control point registration. The running time difference will be more pronounced when the image size is further increased because the running time of DL networks would increase at a much lower ratio thanks to the batch processing power of DL.

To further demonstrate the matching quality of the proposed method, we adopted the gray level residual (GLR) field [33–35], which reflects match quality and highlights mismatched areas with intuitive visual cues. Fig. 13(a) represents the original reference image. The calculation of the GLR field has been adjusted for the dense displacement obtained by DL-based methods where the deformed image is warped by the dense displacement fields, as shown in Fig. 13(b). As shown in Fig. 13(c), the GLR field only considers the displacement correction and keeps the residuals of lighting variation, which could help to identify the

Fig. 13 (a) reference image, (b) deformed image with displacement correction and (c) gray level residual field of the matching result



residuals of different types. In the GLR field, residuals in most areas are at a low level and areas with high residuals have been marked out. Residuals in the upper part, caused by illumination variation, are smoothly distributed and lower than 50 grayscales. In the lower part, highlights caused by reflective light are observed in both the reference and deformed images. These highlights may lead to residuals greater than 100 grayscales. Both the lighting variation and highlights may cause errors for DL-based methods if these factors are not included in the dataset. However, in this work, the adopted improved RAFT trained with a dataset of high-quality shows reliable performance in this challenging task, proving the robustness and practicality of the proposed method in real-world experiments.

Conclusions and future works

This work proposes an improved DL-based DIC method using the idea of the domain decomposition method, which greatly extends the robustness and practicality of existing DL-based DIC. The proposed method decomposes the DIC matching problem into two stages, i.e., large deformation removal and small deformations extraction. The ROI is divided into subimages using the pre-registered control points, then the large deformation is removed by perspective transformation. The residual small deformation can be easily extracted with the existing DL-based method. The proposed method has several advantages:

1. The proposed method can be applied in real-world experiments that would involve large deformations. It removes the large deformations and standardizes the local problems into subimages with fixed input size and limited deformation. It brings the same adaptability and applicability as the standard local DIC method and the same accuracy and efficiency as the DL-based methods. The proposed method can obtain full field pixelwise results in general measurement tasks without sacrificing accuracy in small deformation. It also reduces the cost of memory and computer resources, breaking the limitations of existing DL-based methods.
2. The proposed method contains two stages and is composable, different initial value estimation methods and DL-based methods can be used in the proposed method. It extends the application ranges of existing DL-based networks to real-world experiment scenarios without complex modification and retraining, improving the general applicability of existing DL-based methods.

Future work can be carried out in the following aspects. First, new DL networks can be tested and optimized on

standardized local problems to realize higher accuracy and adaptability. Second, a DL-based initial value estimation method for large displacement can be adopted to realize an end-to-end DL-based DIC solution. Third, the proposed DDM strategy is not exclusive to DL-based methods. The local problems can also be solved with traditional methods such as local DIC or global DIC, and they can also benefit from the advantages offered by the DDM strategy.

Acknowledgments This work is supported by the National Natural Science Foundation of China (Grant nos. 11925202). National Science and Technology Major Project (J2019-V-0006-0099).

Data Availability The data that support the findings of this study are available from the corresponding author upon reasonable request.

Declarations

Conflict of interest The authors have no competing interests to declare that are relevant to the content of this article.

Reference

1. Pan B, Qian K, Xie H, Asundi A (2009) Two-dimensional digital image correlation for in-plane displacement and strain measurement: a review. *Measure Sci Technol* 20:062001. <https://doi.org/10.1088/0957-0233/20/6/062001>
2. Pan B (2018) Digital image correlation for surface deformation measurement: historical developments, recent advances and future goals. *Meas Sci Technol* 29:082001. <https://doi.org/10.1088/1361-6501/aac55b>
3. Schreier H, Orteu J-J, Sutton MA (2009) *Image Correlation for Shape, Motion and Deformation Measurements: Basic Concepts, Theory and Applications*. Springer US, Boston, MA
4. Bruck HA, McNeill SR, Sutton MA, Peters WH (1989) Digital image correlation using Newton-Raphson method of partial differential correction. *Exp Mech* 29:261–267. <https://doi.org/10.1007/BF02321405>
5. Lu H, Cary PD (2000) Deformation measurements by digital image correlation: Implementation of a second-order displacement gradient. *Exp Mech* 40:393–400. <https://doi.org/10.1007/BF02326485>
6. Sun Y, Pang JH, Wong CK, Su F (2005) Finite element formulation for a digital image correlation method. *Applied Optics* 44:7357–7363. <https://doi.org/10.1364/AO.44.007357>
7. Besnard G, Hild F, Roux S (2006) “Finite-Element” Displacement Fields Analysis from Digital Images: Application to Portevin–Le Châtelier Bands. *Exp Mech* 46:789–803. <https://doi.org/10.1007/s11340-006-9824-8>
8. Ma S, Zhao Z, Wang X (2012) Mesh-based digital image correlation method using higher order isoparametric elements. *J Strain Analys Eng Des* 47:163–175. <https://doi.org/10.1177/0309324712437488>
9. Wittevrongel L, Lava P, Lomov SV, Debruyne D (2015) A Self Adaptive Global Digital Image Correlation Algorithm. *Exp Mech* 55:361–378. <https://doi.org/10.1007/s11340-014-9946-3>
10. Hornik K (1991) Approximation capabilities of multilayer feedforward networks. *Neural Netw* 4:251–257. [https://doi.org/10.1016/0893-6080\(91\)90009-T](https://doi.org/10.1016/0893-6080(91)90009-T)
11. Boukhtache S, Abdelouahab K, Berry F et al (2021) When Deep Learning Meets Digital Image Correlation. *Optics Lasers Eng* 136:106308. <https://doi.org/10.1016/j.optlaseng.2020.106308>

12. Boukhtache S, Abdelouahab K, Bahou A et al (2023) A lightweight convolutional neural network as an alternative to DIC to measure in-plane displacement fields. *Optics Lasers Eng* 161:107367. <https://doi.org/10.1016/j.optlaseng.2022.107367>
13. Ronneberger O, Fischer P, Brox T (2015) U-Net: Convolutional Networks for Biomedical Image Segmentation. In: Navab N, Hornegger J, Wells WM, Frangi AF (eds) *Medical Image Computing and Computer-Assisted Intervention – MICCAI 2015*. Springer International Publishing, Cham, pp 234–241
14. Dosovitskiy A, Fischer P, Ilg E et al (2015) FlowNet: Learning Optical Flow with Convolutional Networks. In: 2015 IEEE International Conference on Computer Vision (ICCV). 2758–2766
15. Sun D, Yang X, Liu M-Y, Kautz J (2018) PWC-Net: CNNs for Optical Flow Using Pyramid, Warping, and Cost Volume. In: 2018 IEEE/CVF Conference on Computer Vision and Pattern Recognition. 8934–8943
16. Yang R, Li Y, Zeng D, Guo P (2022) Deep DIC: Deep learning-based digital image correlation for end-to-end displacement and strain measurement. *J Mater Proc Technol* 302:117474. <https://doi.org/10.1016/j.jmatprotec.2021.117474>
17. Wang Y, Zhao J (2023) DIC-Net: Upgrade the performance of traditional DIC with Hermite dataset and convolution neural network. *Optics Lasers in Engineering* 160:107278. <https://doi.org/10.1016/j.optlaseng.2022.107278>
18. Xiao H, Li C, Feng M (2023) Large Deformation Measurement Method of Speckle Images Based on Deep Learning. *Acta Optica Sinica* 43:1–13. <https://doi.org/10.3788/AOS222084>
19. Ma C, Ren Q, Zhao J (2021) Optical-numerical method based on a convolutional neural network for full-field subpixel displacement measurements. *Opt Express* 29:9137. <https://doi.org/10.1364/OE.417413>
20. Duan X, Huang J (2022) Deep learning-based digital volume correlation. *Extreme Mech Lett* 53:101710. <https://doi.org/10.1016/j.eml.2022.101710>
21. Duan X, Huang J (2022) Deep-learning-based 3D cellular force reconstruction directly from volumetric images. *Biophys J* 121:2180–2192. <https://doi.org/10.1016/j.bpj.2022.04.028>
22. Duan X, Xu H, Dong R et al (2023) Digital image correlation based on convolutional neural networks. *Optics Lasers Eng* 160:107234. <https://doi.org/10.1016/j.optlaseng.2022.107234>
23. Yang J, Qian K, Wang L (2024) R³-DICnet: an end-to-end recursive residual refinement DIC network for larger deformation measurement. *Opt Express* 32:907. <https://doi.org/10.1364/OE.505655>
24. Hui T-W, Tang X, Loy CC (2018) LiteFlowNet: A Lightweight Convolutional Neural Network for Optical Flow Estimation. In: 2018 IEEE/CVF Conference on Computer Vision and Pattern Recognition. 8981–8989
25. Teed Z, Deng J (2020) RAFT: Recurrent All-Pairs Field Transforms for Optical Flow. In: Vedaldi A, Bischof H, Brox T, Frahm J-M (eds) *Computer Vision – ECCV 2020*. Springer International Publishing, Cham, pp 402–419
26. Wang G, Zhang L, Yao X (2022) StrainNet-3D: Real-time and robust 3-dimensional speckle image correlation using deep learning. *Optics Lasers Eng* 158:107184. <https://doi.org/10.1016/j.optlaseng.2022.107184>
27. Toselli A, Widlund OB (2005) *Domain decomposition methods—algorithms and theory*. Springer, Berlin
28. Dolean V, Jolivet P, Nataf F (2015) *An Introduction to Domain Decomposition Methods: Algorithms, Theory, and Parallel Implementation*. Society for Industrial and Applied Mathematics, Philadelphia, PA
29. Passieux J-C, Périé J-N, Salaün M (2015) A dual domain decomposition method for finite element digital image correlation. *Int J Numerical Meth Eng* 102:1670–1682. <https://doi.org/10.1002/nme.4868>
30. Chi Y, Pan B (2022) Accelerating parallel digital image correlation computation with feature mesh interpolation. *Measurement* 199:111554. <https://doi.org/10.1016/j.measurement.2022.111554>
31. Schreier HW, Sutton MA (2002) Systematic errors in digital image correlation due to undermatched subset shape functions. *Exp Mech* 42:303–310. <https://doi.org/10.1007/BF02410987>
32. Pan B, Xie H, Wang Z et al (2008) Study on subset size selection in digital image correlation for speckle patterns. *Optics Exp* 16:7037–7048
33. Rupil J, Roux S, Hild F, Vincent L (2011) Fatigue microcrack detection with digital image correlation. *J Strain Analys Eng Design* 46:492–509. <https://doi.org/10.1177/0309324711402764>
34. Hild F, Bouterf A, Roux S (2015) Damage measurements via DIC. *Int J Fract* 191:77–105. <https://doi.org/10.1007/s10704-015-0004-7>
35. Chi Y, Zhao W, Pan B (2023) Gray level residual field: an effective metric for pixelwise matching quality evaluation in local digital image correlation. *Measure Sci Technol* 34. <https://doi.org/10.1088/1361-6501/acdbdf>

Publisher's Note Springer Nature remains neutral with regard to jurisdictional claims in published maps and institutional affiliations.

Springer Nature or its licensor (e.g. a society or other partner) holds exclusive rights to this article under a publishing agreement with the author(s) or other rightsholder(s); author self-archiving of the accepted manuscript version of this article is solely governed by the terms of such publishing agreement and applicable law.